Positive quantum Lyapunov exponents in classically regular systems

Saúl Pilatowsky-Cameo,[1] Jorge Chávez-Carlos,[1] Miguel A. Bastarrachea-Magnani,[2]
Pavel Stránský,[3] Sergio Lerma-Hernández,[4] Lea F. Santos,[5] and Jorge G. Hirsch[1]

[1]*Instituto de Ciencias Nucleares, Universidad Nacional Autónoma de México, Apdo. Postal 70-543, C.P. 04510 CDMX, México*
[2]*Department of Physics and Astronomy, Aarhus University, Ny Munkegade, DK-8000 Aarhus C, Denmark.*
[3]*Faculty of Mathematics and Physics, Charles University, V Holešovičkách 2, Prague 180 00, Czech Republic*
[4]*Facultad de Física, Universidad Veracruzana, Circuito Aguirre Beltrán s/n, C.P. 91000 Xalapa, Mexico*
[5]*Department of Physics, Yeshiva University, New York, New York 10016, USA.*

Quantum chaos refers to signatures of classical chaos found in the quantum domain. Recently, it has become common to equate the exponential behavior of the quantum evolution of out-of-time order correlators (OTOCs) with quantum chaos. The quantum-classical correspondence between the OTOC exponential growth and chaos in the classical limit has indeed been corroborated for different chaotic systems. In this work, however, we show that OTOCs can grow exponentially also in regular models. This happens when the classical system exhibits isolated unstable points. In the quantum domain, these points become finite regions, where the quantum Lyapunov exponents are throughout positive. Our results are illustrated for the Lipkin-Meshkov-Glick (LMG) model, which is integrable, and for the Dicke Hamiltonian in the regular regime. These models are currently realized in various experimental setups, such as those with cold atoms and ion traps.

Classical chaos in Hamiltonian systems is typically defined by means of the sensitive dependence on initial conditions, which leads to positive Lyapunov exponents (LEs) [1]. But this alone is not a complete definition of chaos. Consider, for example, the simple pendulum. Its upright position corresponds to a stationary point that is unstable. It has a positive LE, as any genuine chaotic system, although it is completely integrable. The lack of chaos in this case is related with the isolation of this point. No other initial condition can reach it, so the pendulum cannot exhibit chaotic behaviors, such as non-periodicity and mixing [2]. In this work, we investigate what happens to such isolated unstable points in the quantum domain.

It was argued in [3] that quantum mechanics can bring chaos to classical systems that are non-chaotic. This idea was inspired by Ref. [4], where a standard non-chaotic classical billiard became chaotic when the point particle was substituted by a finite-size hard sphere. By making a parallel between the semiclassical dynamics of a quantum wave packet and the motion of a finite-size classical particle, it was shown in [3] that quantum chaos can emerge in regular classical billiards. Quantum chaos in this case refers to the exponentially fast growth of the out-of-time ordered correlator (OTOC) at short times.

The OTOC quantifies the degree of non-commutativity in time between two operators. It was introduced in the context of superconductivity [5] to measure the instability of the trajectories of electrons scattered by impurities in the superconductor. Recently, the OTOC became a key quantity in definitions of many-body quantum chaos [6–14], analysis of the quantum-classical correspondence of chaotic systems [15–24], and studies of the scrambling of quantum information [25, 26] and quantum phase transitions [27, 28]. The OTOC has been measured experimentally with ion traps [29] and nuclear magnetic resonance platforms [30–32].

Depending on how the OTOC is computed, it may be called microcanonical OTOC (MOTOC) [18], fidelity OTOC (FO-

TOC) [26], thermal OTOC [8], and OTOC for specific initial states [3, 16]. The exponential growth rate of the latter, of the MOTOC [19], and of the FOTOC [26] was shown to be related with the classical LE of chaotic systems. This justifies referring to the OTOCs exponential growth rates as quantum LEs and associating their exponential behavior with the notion of quantum chaos.

Here, we study the FOTOC in systems that are classically regular and have isolated unstable points of measure zero. Due to the uncertainty principle, such isolated points become finite regions in the quantum domain. As a result, we find that the FOTOC grows exponentially not only for initial states centered at the classically isolated unstable point, but also for states centered at the surrounding points. This is entirely at odds with the classical limit, where for initial conditions in the surrounding region of zero classical LEs, the unstable point is inaccessible. Quantum mechanics therefore generates instability in a region where the classical dynamics is stable. Following the current terminology, we then refer to these regions as "quantum chaotic", although one may ponder whether, similarly to the above discussion about classical chaos, additional conditions, on top of the exponential growth of the OTOCs, are also needed for defining quantum chaos.

We analyze the evolution of the FOTOC in the Lipkin-Meshkov-Glick (LMG) Hamiltonian and in the regular regime of the Dicke Hamiltonian. The LMG model is a one-dimensional classically integrable system introduced in nuclear physics [33] and realized experimentally with cold atoms [34, 35] and nuclear magnetic resonance platforms [36]. The Dicke model is a two-dimensional non-integrable model used to describe strongly interacting light-matter systems [37–39]. It presents chaotic and regular regimes, and has been realized experimentally with cold atoms [40–43], by means of cavity Raman transitions [44, 45], and with ion traps [46]. The latter is a promising experimental setup for measuring the FOTOC.

The unstable points of the LMG and Dicke models.– In a

classical Hamiltonian system with real first-order differential equations $d\boldsymbol{x}/dt = \boldsymbol{\mathcal{F}}(\boldsymbol{x})$, where $\boldsymbol{x} = (\boldsymbol{q}, \boldsymbol{p})$ are the generalized coordinates and momenta, a point $\boldsymbol{x} = \boldsymbol{x}_0$ is stationary when $\boldsymbol{\mathcal{F}}(\boldsymbol{x}_0) = 0$. This point is unstable when at least one of the positive-negative pairs of eigenvalues of the Jacobian matrix of $\boldsymbol{\mathcal{F}}$ evaluated at $\boldsymbol{x}_0$ has a nonzero real part. The LE of this point equals the maximum of these real part values [see the Supplemental Material (SM) in [47] for more details]. Both the LMG and the Dicke model in the classical limit present stationary points with positive LEs.

The LMG model [33] describes the collective motion of a set of N two-level systems mutually interacting. Its quantum Hamiltonian is given by

$$\hat{H}_{\text{LMG}} = \Omega \hat{J}_z + \frac{\xi}{j} \hat{J}_x^2, \tag{1}$$

where $\hbar = 1$, Ω is the energy difference of the two-level systems, ξ is the coupling strength, $\hat{J}_{x,y,z} = (1/2) \sum_{n=1}^{N} \sigma_{x,y,z}^{(n)}$ are the collective pseudo-spin operators given by the sum of Pauli matrices $\sigma_{x,y,z}^{(n)}$ for each two-level system n, and $j = N/2$, where j comes from the eigenvalue $j(j+1)$ of the total spin operator $\hat{\boldsymbol{J}}^2 = \hat{J}_x^2 + \hat{J}_y^2 + \hat{J}_z^2$ and thus gives the size of the system. This model has been employed, for example, in studies of ground state quantum phase transitions (QPTs) and excited state quantum phase transitions (ESQPTs) [48–51], entanglement [52, 53], and quantum speed limit [54].

The classical LMG Hamiltonian is obtained by taking the expectation value of $\hat{H}_{\text{LMG}}/j$ on Bloch coherent states $|z\rangle = \left(1 + |z|^2\right)^{-j} e^{z\hat{J}_+} |j, -j\rangle$, where $|j, -j\rangle$ is the state with the lowest pseudo-spin projection, and $\hat{J}_+$ is the raising operator. Defining z in terms of the canonical variables (Q, P) as $z = (Q - iP)/\sqrt{4 - (Q^2 + P^2)}$ and neglecting $\mathcal{O}(1/j)$ terms, the classical LMG Hamiltonian reads

$$H_{\text{LMG}}(Q,P) = \frac{\Omega}{2}\left(Q^2 + P^2\right) - \Omega + \xi\left(Q^2 - \frac{Q^2 P^2}{4} - \frac{Q^4}{4}\right). \tag{2}$$

The Hamiltonian (2) is regular, but its stationary point $\boldsymbol{x}_0 = (Q = 0, P = 0)$ is unstable and presents a positive LE given by (see SM [47]),

$$\lambda = \sqrt{-(\Omega^2 + 2\Omega\xi)}, \tag{3}$$

when $\Omega < -2\xi$. Figures 1 (a) and (b) show the energy surface of the classical LMG model for two values of Ω and $\xi = -1$. When $\Omega \geq -2\xi$, $\boldsymbol{x}_0$ is a minimum, while for $\Omega < -2\xi$, $\boldsymbol{x}_0$ becomes a saddle point and therefore unstable.

This saddle point is associated with an ESQPT in the quantum domain. A main signature of ESQPTs is the divergence of the density of states at an energy denoted by E_{ESQPT}. In the mean-field approximation, it has been shown that this energy coincides with the energy of the classical system at the saddle point [48, 55], that is, for the LMG model, $E_{\text{ESQPT}}^{\text{LMG}}/j = H_{\text{LMG}}(\boldsymbol{x}_0) = -\Omega$.

The Dicke model is a collection of N two-level atoms of level spacing ω_0 coupled to a quantized radiation field of fre-
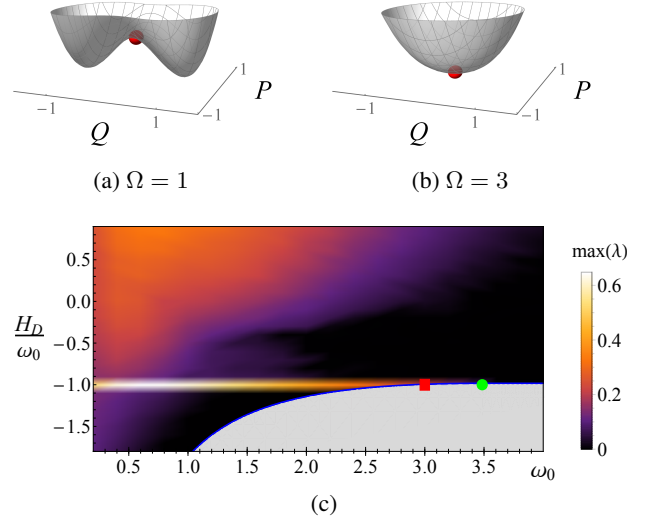

(a) $\Omega = 1$ (b) $\Omega = 3$

(c)

Figure 1. Top: Energy surface for the classical LMG model for two values of the parameter Ω fixing $\xi = -1$. The stationary point $\boldsymbol{x}_0 = (Q = 0, P = 0)$ is marked with a red sphere. It is a saddle point for $\Omega = 1$ (a) and a minimum for $\Omega = 3$ (b). Panel (c): Each colored point corresponds to the maximal classical Lyapunov exponent for the Dicke model in a plane resulting from the intersection of an energy shell (with energy indicated by the vertical axis) and the hyperplane $p = 0$. This is done for different values of ω_0 as indicated by the horizontal axis. We fix $\gamma = 0.66$ and $\omega = 0.5$. The red square at $\omega_0 = 3$ is the unstable point studied in Fig. 3. The green circle at $\omega_{0c} = 3.48$ is the critical point that marks the ground state quantum phase transition.

quency ω. In the symmetric atomic subspace, the Hamiltonian is given by

$$\hat{H}_D = \frac{\omega}{2}(\hat{q}^2 + \hat{p}^2) + \omega_0 \hat{J}_z + 2\frac{\gamma}{\sqrt{j}}\hat{J}_x\,\hat{q} - \frac{\omega}{2}, \tag{4}$$

where $\hat{q} = (\hat{a}^\dagger + \hat{a})/\sqrt{2}$ and $\hat{p} = i(\hat{a}^\dagger - \hat{a})/\sqrt{2}$, with $\hat{a}(\hat{a}^\dagger)$ being the annihilation (creation) operator, and γ is the atom-field interaction strength. As in the LMG model, $j = N/2$ gives the system size.

The Dicke model was first used to explain the collective phenomenon of superradiance [37, 56]. It is now used in studies of QPTs and ESQPTs [56–61], quantum chaos [62–65], monodromy [66, 67], entanglement creation [68], nonequilibrium dynamics [69–73], the OTOC behavior [26, 74], and quantum batteries [75].

The classical Dicke Hamiltonian [65, 76, 77] is obtained by taking the expectation value of $\hat{H}_D/j$ between the product of Bloch coherent states and Glauber coherent states $|\alpha\rangle = e^{-|\alpha|^2/2}e^{\alpha\hat{a}^\dagger}|0\rangle$, where $\alpha = \sqrt{j/2}(q + ip) \in \mathbb{C}$, and $|0\rangle$ is the photon vacuum. In terms of the canonical variables (Q, P) for the pseudo-spin and of (q, p) for the field [47], it reads

$$H_D = \frac{\omega}{2}\left(q^2 + p^2\right) - \omega_0 + \frac{\omega_0}{2}\left(Q^2 + P^2\right)$$
$$+ 2\gamma\sqrt{1 - \frac{1}{4}\left(Q^2 + P^2\right)}\,q\,Q. \tag{5}$$

The stationary point of the Dicke model is $\boldsymbol{x}_0 = (q = 0, p = 0, Q = 0, P = 0)$. The LE associated with it can be calculated in terms of ω, ω_0 and γ, as (see SM [47])

$$\lambda = \frac{1}{\sqrt{2}} \sqrt{-(\omega^2 + \omega_0^2) + \sqrt{(\omega^2 - \omega_0^2)^2 + 16\gamma^2 \omega \omega_0}}. \quad (6)$$

When $\omega_0 < \omega_{0c} = 4\gamma^2/\omega$, this equation gives a positive value for the LE and the stationary point is unstable. When $\omega_0 > \omega_{0c}$, Eq. (6) has pure imaginary values and the LE is zero. The point ω_{0c} marks the ground state QPT of the Dicke model. For $\omega_0 < \omega_{0c}$, the system is in the superradiant phase, and for $\omega_0 > \omega_{0c}$, it is in the normal phase. The unstable point is therefore in the superradiant phase.

Energy surfaces similar to those in Figs. 1 (a) and (b) can also be drawn for the Dicke model, but in higher dimension. The saddle point of this model is also associated with an ES-QPT [60], which happens at $E_{\text{ESQPT}}^{\text{D}}/j = H_D(\boldsymbol{x}_0) = -\omega_0$. We stress that, contrary to common belief, the ESQPT in the Dicke model is not directly related with the transition to classical chaos [65, 78].

In Fig. 1 (c), we show the largest LEs of the Dicke model as functions of the classical excitation energy H_D/ω_0 and of the atomic frequency ω_0, for $\gamma = 0.66$ and $\omega = 0.5$. Employing frequency units of kHz/2π, these values coincide with those used in the experiment with ion traps [26, 46]. The thick blue line in the figure depicts the ground state energy and the gray area under it is forbidden. The color gradient indicates presence or absence of chaos: black represents regular regions and light areas have large LEs. The bright horizontal line at the ESQPT, $H_D/\omega_0 = -1$, indicates very large LEs and reflects the instability.

According to Eq. (6), the maximum LE is obtained for $\omega_0 = 0.649$, which is approximately the value used in [26]. As one sees in Fig. 1 (c), this classical instability is immersed in a chaotic region of the phase space with positive LEs, so we show some results for it only in the SM [47]. Here, our main focus is on the unstable point at $\omega_0 = 3$, which is marked in the figure with a red square. The area surrounding this point is completely regular, with zero LEs throughout [65]. This is the point that we use in our studies in Fig. 3. But before showing those results, let us describe how the quantum and classical evolutions are carried out and compared.

Quantum-classical correspondence.– The OTOC measures the degree of non-commutativity in time between operators $\hat{W}$ and $\hat{V}$, $O_{toc}(t) = -\langle [\hat{W}(t), \hat{V}(0)]^2 \rangle$. It is known as FOTOC when $\hat{W} = e^{i\delta\phi\hat{G}}$, where $\hat{G}$ is a Hermitian operator and $\delta\phi$ is a small perturbation, and $\hat{V} = |\Psi_0\rangle\langle\Psi_0|$ is the projection operator onto the initial state. In the perturbative limit, $\delta\phi \ll 1$, the dynamics of the FOTOC agrees with that of the variance of $\hat{G}$ ([26], see also SM [47]),

$$\sigma_G^2(t) = \langle \hat{G}^2(t) \rangle - \langle \hat{G}(t) \rangle^2, \quad (7)$$

so we refer to this variance as FOTOC and denote its exponential growth rate by 2Λ. In what follows, we refer to Λ as the quantum LE.

The FOTOC enables a direct visualization of the quantum evolution in terms of the dynamics in phase space. It measures the spread of the size of the wave packet and can thus be compared with the variance of the canonical variables in phase space. A great advantage of the FOTOC is that it can be computed with semiclassical phase-space methods, such as the truncated Wigner approximation (TWA) [79–81], which makes accessible system sizes that are not achievable with exact diagonalization. This is particularly useful for the Dicke model, which is non-integrable and where the number of bosons in the field is not limited.

The basic idea of the TWA [80] is to compute the dynamics using the classical equations of motion, but averaging the observable over a large sample of initial conditions and replacing the classical probability distribution with the Wigner function [82] and the classical observable with the Weyl symbol of the corresponding quantum operator [83]. The random sampling reproduces the quantum fluctuations of a quantum initial state.

To compute the FOTOC, we consider initial Bloch coherent states for the LMG model, and initial products of Bloch and Glauber coherent states for the Dicke model. This implies that the initial Wigner functions are positive and approximately given by normal distributions. Our sampling is done by means of a Monte Carlo method [81] over $\sim 10^4$ random points (see details in SM [47]).

In Fig. 2, we compare the quantum LE obtained for the FOTOC with the classical LE for the LMG (a) and the Dicke (b) model at an unstable point. For the LMG model, the quantum evolution is done exactly. Since the wave packet spreads in both directions in phase space, we analyze the growth of $\sigma_Q^2(t) + \sigma_P^2(t)$. The agreement between λ from Eq. (3) and Λ is perfect.

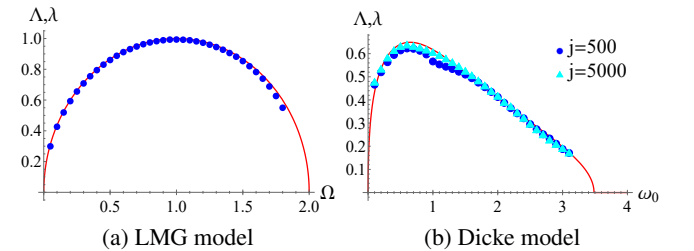(a) LMG model   (b) Dicke model

Figure 2. The classical LE λ (solid line) and the quantum LE Λ (symbols) for the LMG (a) and the Dicke (b) model at the stationary point. The results for Λ for the LMG model are obtained with the exact quantum evolution and for the Dicke model, the TWA is used. For the LMG model, the FOTOC corresponds to $\sigma_Q^2(t) + \sigma_P^2(t)$, $\xi = -1$, and $j = 500$. For the Dicke model, the FOTOC is $\sigma_Q^2(t) + \sigma_P^2(t) + \sigma_q^2(t) + \sigma_p^2(t)$, $\omega = 0.5$, $\gamma = 0.66$, and the j's are indicated.

For the Dicke model, we study $\sigma_Q^2(t) + \sigma_P^2(t) + \sigma_q^2(t) + \sigma_p^2(t)$. Employing an efficient basis for the convergence of the eigenstates [84], we evaluated the exact quantum evolution for $j = 100$, where the truncated Hilbert space has 24 453 converged eigenstates. We verified that for this size, which is already large for exact diagonalization, the exact quantum evo-

lution and the evolution done with the TWA agree extremely well from $t = 0$ up to times beyond the exponential growth of the FOTOC (see SM [47]). This assures us that we can use the TWA to calculate Λ for $j = 500$ and $j = 5000$. As one increases j, the agreement between λ from Eq. (6) and the quantum LE improves, as seen in Fig. 2 (b).

Quantum activation of the instability.– The results above make evident that, despite the regularity of the systems, both classical and quantum LEs coincide and are positive at the unstable points. We now investigate what happens at the vicinity of the unstable point of the LMG model with $\Omega = 1$ and of the Dicke model with $\omega_0 = 3$. Classically, the LEs in the surrounding region are zero and the unstable point is simply unreachable. To analyze what happens in the quantum domain, we study the behavior of the FOTOC as one moves away from the unstable point.
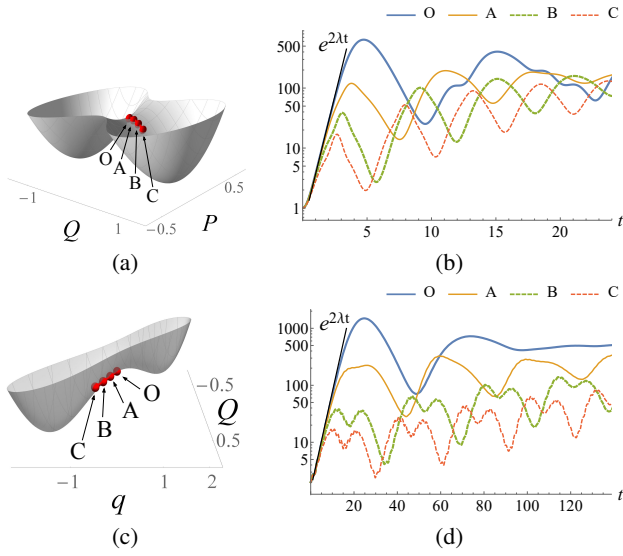

(a)

(b)

(c)

(d)

Figure 3. Energy surface of the LMG model (a) and of the Dicke model with $P = p = 0$ (c), and FOTOC behavior for the LMG model, $\sigma_Q^2(t) + \sigma_P^2(t)$, (b) and for the Dicke model, $\sigma_Q^2(t) + \sigma_P^2(t) + \sigma_q^2(t) + \sigma_p^2(t)$, (d). The FOTOC is computed for coherent states centered at the unstable point O and around it, at points A, B, and C. The (black) straight line in (b) and (d) corresponds to the exponential curve with rate given by twice the classical LE. The initial growth rate of the FOTOC for all points and for both models is $2\Lambda \approx 2\lambda$. For the LMG model: $\xi = -1$, $\Omega = 1$, $j = 500$, and the points A, B, and C have constant $P = 0$ and $Q = 0.1, 0.2, 0.3$, respectively. For the Dicke model: $\omega = 0.5$, $\gamma = 0.66$, $\omega_0 = 3$, and $j = 500$. The points A, B, and C have $P = p = 0$, $Q = 0.1, 0.2$, and 0.3, respectively, and q is chosen so that $H_D = -\omega_0$ for all four points.

The unstable point is marked as O in the energy surface of the LMG model in Fig. 3 (a) and of the Dicke model in Fig. 3 (c). Points O, A, B, and C correspond to the center of the coherent states used in the calculation of the FOTOC. The choices of A, B, and C are done such that the trajectories do not go (come) asymptotically to (from) the unstable point. To guarantee this, since the LMG model has only one degree of freedom, the points A, B, and C have decreasing energies,

while for the Dicke model, it is enough to select different values of Q with the same energy $H_D = -\omega_0$.

For any of the points (and for those in between them), the initial evolution of the FOTOC is exactly the same as the one for O, with the same exponential growth rate $2\Lambda \approx 2\lambda$, as clearly seen in Fig. 3 (b) [Fig. 3 (d)] for the LMG [Dicke] model. What changes is the duration of the exponential behavior, which becomes shorter as one gets further from O, and also the saturation value of the dynamics, which gets lower and shows larger oscillations.

Figure 3 demonstrates that, in absolute contrast with the classical dynamics, quantum instability is not only possible, but is ubiquitous in the vicinity of an unstable point. One needs to move quite far from the unstable point for getting rid of any reminiscence of an exponential growth.

Discussion.– Classical systems in the regular regime, as the LMG and the Dicke model considered here, can exhibit unstable points with positive LEs. This reflects on the onset of positive quantum LEs for initial states centered at those same points. Classically, these unstable points have measure zero, being surrounded by points with zero LEs. In the quantum domain, on the other hand, these points become finite regions, where the exponential behavior of the FOTOC is throughout verified. Quantum mechanics can therefore activate instability in regions where the classical dynamics is not unstable. In these regions, the quantum-classical correspondence does not hold even at very short times. We leave as an open question whether these systems should indeed be called "chaotic quantum systems". A positive answer would imply detaching the concept of quantum chaos from the presence of chaos in the classical limit.

[1] Edward Ott, "Chaos in Dynamical Systems" (Cambridge University Press, Cambridge, 2002).

[2] Pierre Gaspard, "Chaos, scattering and statistical mechanics" (Cambridge University Press, 1998).

[3] Efim B. Rozenbaum, Leonid A. Bunimovich, and Victor Galitski, "Quantum chaos in classically non-chaotic systems," arXiv:1902.05466.

[4] L.A. Bunimovich, "Physical versus mathematical billiards: From regular dynamics to chaos and back," ArXiv:1903.02634.

[5] A. Larkin and Yu. N. Ovchinnikov, Zh. Eksp. Teor. Fiz. 55, 2262 (1969) ["Quasiclassical Method in the Theory of Superconductivity", Sov. Phys. JETP **28**, 1200 (1969)].

[6] A. Kitaev, "Kitp talk," Http://online.kitp.ucsb.edu/online/entan-gled15/kitaev/.

[7] Juan Maldacena and Douglas Stanford, "Remarks on the Sachdev-Ye-Kitaev model," Phys. Rev. D **94**, 106002 (2016).

[8] Juan Maldacena, Stephen H. Shenker, and Douglas Stanford, "A bound on chaos," J. High Energy Phys. **2016**, 106 (2016).

[9] Daniel A. Roberts and Douglas Stanford, "Diagnosing chaos using four-point functions in two-dimensional conformal field theory," Phys. Rev. Lett. **115**, 131603 (2015).

[10] Ruihua Fan, Pengfei Zhang, Huitao Shen, and Hui Zhai, "Out-of-time-order correlation for many-body localization," Science Bulletin **62**, 707 – 711 (2017).

[11] David J. Luitz and Yevgeny Bar Lev, "Information propagation in isolated quantum systems," Phys. Rev. B **96**, 020406 (2017).

[12] E. J. Torres-Herrera, Antonio M. García-García, and Lea F. Santos, "Generic dynamical features of quenched interacting quantum systems: Survival probability, density imbalance, and out-of-time-ordered correlator," Phys. Rev. B **97**, 060303 (2018).

[13] Fausto Borgonovi, Felix M. Izrailev, and Lea F. Santos, "Timescales in the quench dynamics of many-body quantum systems: Participation ratio versus out-of-time ordered correlator," Phys. Rev. E **99**, 052143 (2019).

[14] Hua Yan, Jiaozi Wang, and Wen ge Wang, "Similar early growth of out-of-time-ordered correlators in quantum chaotic and integrable ising chains," ArXiv:1906.11775.

[15] T. A. Elsayed and B. V. Fine, Sensitivity to small perturbations in systems of large quantum spins, Phys. Scr. **T165**, 014011 (2015).

[16] Efim B. Rozenbaum, Sriram Ganeshan, and Victor Galitski, "Lyapunov exponent and out-of-time-ordered correlator's growth rate in a chaotic system," Phys. Rev. Lett. **118**, 086801 (2017).

[17] E. B. Rozenbaum, S. Ganeshan, and V. Galitski, "Universal level statistics of the out-of-time-ordered operator," (), arXiv:1801.10591.

[18] Koji Hashimoto, Keiju Murata, and Ryosuke Yoshii, "Out-of-time-order correlators in quantum mechanics," J. High Energy Phys. **2017**, 138 (2017).

[19] Jorge Chávez-Carlos, B. López-del Carpio, Miguel A. Bastarrachea-Magnani, Pavel Stránský, Sergio Lerma-Hernández, Lea F. Santos, and Jorge G. Hirsch, "Quantum and classical Lyapunov exponents in atom-field interaction systems," Phys. Rev. Lett. **122**, 024101 (2019).

[20] Ignacio García-Mata, Marcos Saraceno, Rodolfo A. Jalabert, Augusto J. Roncaglia, and Diego A. Wisniacki, "Chaos signatures in the short and long time behavior of the out-of-time ordered correlator," Phys. Rev. Lett. **121**, 210601 (2018).

[21] Rodolfo A. Jalabert, Ignacio García-Mata, and Diego A. Wisniacki, "Semiclassical theory of out-of-time-order correlators for low-dimensional classically chaotic systems," Phys. Rev. E **98**, 062218 (2018).

[22] Emiliano M. Fortes, Ignacio García-Mata, Rodolfo A. Jalabert, and Diego A. Wisniacki, "Gauging classical and quantum integrability through out-of-time ordered correlators," ArXiv:1906.07706.

[23] Josef Rammensee, Juan Diego Urbina, and Klaus Richter, "Many-body quantum interference and the saturation of out-of-time-order correlators," Phys. Rev. Lett. **121**, 124101 (2018).

[24] Arul Lakshminarayan, "Out-of-time-ordered correlator in the quantum bakers map and truncated unitary matrices," Phys. Rev. E **99**, 012201 (2019).

[25] Martin Gärttner, Philipp Hauke, and Ana Maria Rey, "Relating out-of-time-order correlations to entanglement via multiple-quantum coherences," Phys. Rev. Lett. **120**, 040402 (2018).

[26] R. J. Lewis-Swan, A. Safavi-Naini, J. J. Bollinger, and A. M. Rey, "Unifying scrambling, thermalization and entanglement through measurement of fidelity out-of-time-order correlators in the Dicke model," Nat. Comm. **10**, 1581 (2019).

[27] Huitao Shen, Pengfei Zhang, Ruihua Fan, and Hui Zhai, "Out-of-time-order correlation at a quantum phase transition," Phys. Rev. B **96**, 054503 (2017).

[28] Qian Wang and Francisco Pérez-Bernal, "Probing excited-state quantum phase transition in a quantum many body system via out-of-time-ordered correlator," ArXiv:1812.01920.

[29] Martin Gärttner, Justin G. Bohnet, Arghavan Safavi-Naini, Michael L. Wall, John J. Bollinger, and Ana Maria Rey, "Measuring out-of-time-order correlations and multiple quantum spectra in a trapped-ion quantum magnet," Nat. Phys. **13**, 781 – 786 (2017).

[30] Jun Li, Ruihua Fan, Hengyan Wang, Bingtian Ye, Bei Zeng, Hui Zhai, Xinhua Peng, and Jiangfeng Du, "Measuring out-of-time-order correlators on a nuclear magnetic resonance quantum simulator," Phys. Rev. X **7**, 031011 (2017).

[31] Ken Xuan Wei, Chandrasekhar Ramanathan, and Paola Cappellaro, "Exploring localization in nuclear spin chains," Phys. Rev. Lett. **120**, 070501 (2018).

[32] Mohamad Niknam, Lea F. Santos, and David G. Cory, "Sensitivity of quantum information to environment perturbations measured with the out-of-time-order correlation function," ArXiv:1808.04375.

[33] H. J. Lipkin, N. Meshkov, and A. J. Glick, "Validity of many-body approximation methods for a solvable model: (i). Exact solutions and perturbation theory," Nucl. Phys. **62**, 188–198 (1965); "Validity of many-body approximation methods for a solvable model: (ii). Linearization procedures," **62**, 199–210 (1965); "Validity of many-body approximation methods for a solvable model: (iii). Diagram summations," **62**, 211–224 (1965).

[34] C. Gross, T. Zibold, E. Nicklas, J. Estève, and M. K. Oberthaler, "Nonlinear atom interferometer surpasses classical precision limit," Nature **464**, 1165–1169 (2010).

[35] Tilman Zibold, Eike Nicklas, Christian Gross, and Markus K. Oberthaler, "Classical bifurcation at the transition from Rabi to Josephson dynamics," Phys. Rev. Lett. **105**, 204101 (2010).

[36] A. G. Araujo-Ferreira, R. Auccaise, R. S. Sarthour, I. S. Oliveira, T. J. Bonagamba, and I. Roditi, "Classical bifurcation in a quadrupolar nmr system," Phys. Rev. A **87**, 053605 (2013).

[37] R. H. Dicke, "Coherence in spontaneous radiation processes," Phys. Rev. **93**, 99 (1954).

[38] Barry M. Garraway, "The Dicke model in quantum optics: Dicke model revisited," Philos. Trans. Royal Soc. A **369**, 1137 (2011).

[39] Peter Kirton, Mor M. Roses, Jonathan Keeling, and Emanuele G. Dalla Torre, "Introduction to the Dicke model: From equilibrium to nonequilibrium, and vice versa," Advanced Quantum Technologies **2**, 1800043 (2019).

[40] Kristian Baumann, Christine Guerlin, Ferdinand Brennecke, and Tilman Esslinger, "Dicke quantum phase transition with a superfluid gas in an optical cavity," Nature (London) **464**, 1301 (2010).

[41] K. Baumann, R. Mottl, F. Brennecke, and T. Esslinger, "Exploring symmetry breaking at the Dicke quantum phase transition," Phys. Rev. Lett. **107**, 140402 (2011).

[42] Helmut Ritsch, Peter Domokos, Ferdinand Brennecke, and Tilman Esslinger, "Cold atoms in cavity-generated dynamical optical potentials," Rev. Mod. Phys. **85**, 553–601 (2013).

[43] J. Klinder, H. Keßler, M. Reza Bakhtiari, M. Thorwart, and A. Hemmerich, "Observation of a superradiant mott insulator in the Dicke-Hubbard model," Phys. Rev. Lett. **115**, 230403 (2015).

[44] Markus P. Baden, Kyle J. Arnold, Arne L. Grimsmo, Scott Parkins, and Murray D. Barrett, "Realization of the Dicke model using cavity-assisted Raman transitions," Phys. Rev. Lett. **113**, 020408 (2014).

[45] Zhiqiang Zhang, Chern Hui Lee, Ravi Kumar, K. J. Arnold, Stuart J. Masson, A. L. Grimsmo, A. S. Parkins, and M. D. Barrett, "Dicke-model simulation via cavity-assisted Raman transitions," Phys. Rev. A **97**, 043858 (2018).

[46] A. Safavi-Naini, R. J. Lewis-Swan, J. G. Bohnet, M. Gärttner, K. A. Gilmore, J. E. Jordan, J. Cohn, J. K. Freericks, A. M. Rey, and J. J. Bollinger, "Verification of a many-ion simulator of the Dicke model through slow quenches across a phase transition," Phys. Rev. Lett. **121**, 040503 (2018).

[47] See *Supplemental Material* for details.

[48] M.A. Caprio, P. Cejnar, and F. Iachello, "Excited state quantum phase transitions in many-body systems," Ann. of Phys. **323**, 1106 – 1135 (2008).

[49] Pavel Cejnar, Jan Jolie, and Richard F. Casten, "Quantum phase transitions in the shapes of atomic nuclei," Rev. Mod. Phys. **82**, 2155–2212 (2010).

[50] Lea F. Santos and Francisco Pérez-Bernal, "Structure of eigenstates and quench dynamics at an excited-state quantum phase transition," Phys. Rev. A **92**, 050101 (2015).

[51] L. F. Santos, M. Távora, and F. Pérez-Bernal, "Excited-state quantum phase transitions in many-body systems with infinite-range interaction: Localization, dynamics, and bifurcation," Phys. Rev. A **94**, 012113 (2016).

[52] Guifré Vidal, "Efficient simulation of one-dimensional quantum many-body systems," Phys. Rev. Lett. **93**, 040502 (2004).

[53] Sébastien Dusuel and Julien Vidal, "Finite-size scaling exponents of the Lipkin-Meshkov-Glick model," Phys. Rev. Lett. **93**, 237204 (2004).

[54] Qian Wang and Francisco Pérez-Bernal, "Excited-state quantum phase transition and the quantum-speed-limit time," Phys. Rev. A **100**, 022118 (2019).

[55] Pavel Cejnar, Michal Macek, Stefan Heinze, Jan Jolie, and Jan Dobeš, "Monodromy and excited-state quantum phase transitions in integrable systems: collective vibrations of nuclei," J. Phys. A **39**, L515 (2006).

[56] Klaus Hepp and Elliott H Lieb, "On the superradiant phase transition for molecules in a quantized radiation field: the Dicke maser model," Ann. Phys. (N.Y.) **76**, 360 – 404 (1973); Y. K. Wang and F. T. Hioe, "Phase transition in the Dicke model of superradiance," Phys. Rev. A **7**, 831–836 (1973); H.J. Carmichael, C.W. Gardiner, and D.F. Walls, "Higher order corrections to the Dicke superradiant phase transition," Phys. Lett. A **46**, 47 – 48 (1973).

[57] Octavio Castaños, Ramón López-Peña, Jorge G. Hirsch, and Enrique López-Moreno, "Phase transitions and accidental degeneracy in nonlinear spin systems," Phys. Rev. B **72**, 012406 (2005).

[58] P. Pérez-Fernández, A. Relaño, J. M. Arias, P. Cejnar, J. Dukelsky, and J. E. García-Ramos, "Excited-state phase transition and onset of chaos in quantum optical models," Phys. Rev. E **83**, 046208 (2011).

[59] Tobias Brandes, "Excited-state quantum phase transitions in Dicke superradiance models," Phys. Rev. E **88**, 032133 (2013).

[60] M. A. Bastarrachea-Magnani, S. Lerma-Hernández, and J. G. Hirsch, "Comparative quantum and semiclassical analysis of atom-field systems. I. Density of states and excited-state quantum phase transitions," Phys. Rev. A **89**, 032101 (2014).

[61] Jonas Larson and Elinor K Irish, "Some remarks on superradiant phase transitions in light-matter systems," J. Phys. A **50**, 174002 (2017).

[62] C.H Lewenkopf, M.C Nemes, V Marvulle, M.P Pato, and W.F Wreszinski, "Level statistics transitions in the spin-boson model," Phys. Lett. A **155**, 113 – 116 (1991).

[63] Clive Emary and Tobias Brandes, "Quantum chaos triggered by precursors of a quantum phase transition: The Dicke model," Phys. Rev. Lett. **90**, 044101 (2003); "Chaos and the quantum phase transition in the Dicke model," Phys. Rev. E **67**, 066203 (2003).

[64] M. A. Bastarrachea-Magnani, S. Lerma-Hernández, and J. G. Hirsch, "Comparative quantum and semiclassical analysis of atom-field systems. ii. Chaos and regularity," Phys. Rev. A **89**, 032102 (2014); Miguel Angel Bastarrachea-Magnani, Baldemar López del Carpio, Sergio Lerma-Hernández, and Jorge G Hirsch, "Chaos in the Dicke model: quantum and semiclassical analysis," Phys. Scripta **90**, 068015 (2015); M. A. Bastarrachea-Magnani, B. López-del-Carpio, J. Chávez-Carlos, S. Lerma-Hernández, and J. G. Hirsch, "Delocalization and quantum chaos in atom-field systems," Phys. Rev. E **93**, 022215 (2016).

[65] J. Chávez-Carlos, M. A. Bastarrachea-Magnani, S. Lerma-Hernández, and J. G. Hirsch, "Classical chaos in atom-field systems," Phys. Rev. E **94**, 022209 (2016).

[66] O. Babelon, L. Cantini, and B. Douçot, "A semi-classical study of the Jaynes-Cummings model," J. Stat. Mech. **2009**, P07011 (2009).

[67] Michal Kloc, Pavel Stránský, and Pavel Cejnar, "Monodromy in Dicke superradiance," J. Phys. A **50**, 315205 (2017).

[68] S. Schneider and G. J. Milburn, "Entanglement in the steady state of a collective-angular-momentum (Dicke) model," Phys. Rev. A **65**, 042107 (2002); Neill Lambert, Clive Emary, and Tobias Brandes, "Entanglement and the phase transition in single-mode superradiance," Phys. Rev. Lett. **92**, 073602 (2004); Michal Kloc, Pavel Stránský, and Pavel Cejnar, "Quantum phases and entanglement properties of an extended Dicke model," Ann. Phys. **382**, 85 – 111 (2017).

[69] P. Pérez-Fernández, P. Cejnar, J. M. Arias, J. Dukelsky, J. E. García-Ramos, and A. Relaño, "Quantum quench influenced by an excited-state phase transition," Phys. Rev. A **83**, 033802 (2011).

[70] Alexander Altland and Fritz Haake, "Quantum chaos and effective thermalization," Phys. Rev. Lett. **108**, 073601 (2012).

[71] Sergio Lerma-Hernández, Jorge Chávez-Carlos, Miguel A. Bastarrachea-Magnani, Lea F. Santos, and Jorge G. Hirsch, "Analytical description of the survival probability of coherent states in regular regimes," J. Phys. A **51**, 475302 (2018).

[72] S. Lerma-Hernández, D. Villaseñor, M. A. Bastarrachea-Magnani, E. J. Torres-Herrera, L. F. Santos, and J. G. Hirsch, "Dynamical signatures of quantum chaos and relaxation time scales in a spin-boson system," Phys. Rev. E **100**, 012218 (2019).

[73] Michal Kloc, Pavel Stránský, and Pavel Cejnar, "Quantum quench dynamics in Dicke superradiance models," Phys. Rev. A **98**, 013836 (2018).

[74] Yahya Alavirad and Ali Lavasani, "Scrambling in the Dicke model," Phys. Rev. A **99**, 043602 (2019).

[75] Gian Marcello Andolina, Maximilian Keck, Andrea Mari, Vittorio Giovannetti, and Marco Polini, "Quantum versus classical many-body batteries," Phys. Rev. B **99**, 205437 (2019).

[76] A. D. Ribeiro, M. A. M. de Aguiar, and A. F. R. de Toledo Piza, "The semiclassical coherent state propagator for systems with

spin," J. Phys. A **39**, 3085 (2006).

[77] L. Bakemeier, A. Alvermann, and H. Fehske, "Dynamics of the Dicke model close to the classical limit," Phys. Rev. A **88**, 043835 (2013).

[78] A. Relaño, M. A. Bastarrachea-Magnani, and S. Lerma-Hernández, "Approximated integrability of the Dicke model," EPL (Europhys. Lett.) **116**, 50005 (2016).

[79] M. J. Steel and M. J. Collett, "Quantum state of two trapped Bose-Einstein condensates with a Josephson coupling," Phys. Rev. A **57**, 2920–2930 (1998).

[80] Anatoli Polkovnikov, "Phase space representation of quantum dynamics," Ann. Phys. **325**, 1790 – 1852 (2010).

[81] J. Schachenmayer, A. Pikovski, and A. M. Rey, "Many-body quantum spin dynamics with Monte Carlo trajectories on a discrete phase space," Phys. Rev. X **5**, 011022 (2015).

[82] E. Wigner, "On the quantum correction for thermodynamic equilibrium," Phys. Rev. **40**, 749–759 (1932).

[83] H. Weyl, "Quantenmechanik und gruppentheorie," Zeitschrift für Physik **46**, 1–46 (1927).

[84] Miguel A Bastarrachea-Magnani and Jorge G Hirsch, "Efficient basis for the Dicke model: I. Theory and convergence in energy," Phys. Scripta **2014**, 014005 (2014).

Supplementary Material:
Positive quantum Lyapunov exponents in classically regular systems

Saúl Pilatowsky-Cameo[1], Jorge Chávez-Carlos[1], Miguel A. Bastarrachea-Magnani[2], Pavel Stránský[3], Sergio Lerma-Hernández[4], Lea F. Santos[5], and Jorge G. Hirsch[1]

[1]*Instituto de Ciencias Nucleares, Universidad Nacional Autónoma de México, Apdo. Postal 70-543, C.P. 04510 CDMX, México*
[2]*Department of Physics and Astronomy, Aarhus University, Ny Munkegade, DK-8000 Aarhus C, Denmark*
[3]*Faculty of Mathematics and Physics, Charles University, V Holešovičkách 2, Prague 180 00, Czech Republic*
[4]*Facultad de Física, Universidad Veracruzana, Circuito Aguirre Beltrán s/n, C.P. 91000 Xalapa, México*
[5]*Department of Physics, Yeshiva University, New York, New York 10016, USA*

LYAPUNOV EXPONENT FOR STATIONARY POINTS OF CLASSICAL HAMILTONIAN SYSTEMS

In this section we show how to obtain the Lyapunov exponents (LEs) associated with the stationary points of classical systems. Consider a classical Hamiltonian system $H(\boldsymbol{x})$ with n degrees of freedom and a set of generalized coordinates and respective momenta $\boldsymbol{x} = (\boldsymbol{q}, \boldsymbol{p}) = (q_1, ..., q_n, p_1, ...p_n)$. We denote the Hamilton dynamical equations by $\dot{\boldsymbol{x}} = \mathcal{F}(\boldsymbol{x})$. A stationary point $\boldsymbol{x}_0$ of the system satisfies $\mathcal{F}(\boldsymbol{x}_0) = 0$, i.e. $\boldsymbol{x}_0(t) = \boldsymbol{x}_0(t_0)$.

To calculate the LE λ associated with $\boldsymbol{x}_0$, we employ the tangent space by means of the fundamental matrix of the system, $\boldsymbol{\Phi}_{\boldsymbol{x}}(t)$ [1]. This matrix solves the simultaneous equations

$$\begin{pmatrix} \dot{\boldsymbol{x}} \\ \dot{\boldsymbol{\Phi}}_{\boldsymbol{x}} \end{pmatrix} = \begin{pmatrix} \mathcal{F}(\boldsymbol{x}) \\ D_{\boldsymbol{x}}\mathcal{F}(\boldsymbol{x})\boldsymbol{\Phi}_{\boldsymbol{x}} \end{pmatrix}, \qquad \begin{pmatrix} \boldsymbol{x}(t_0) \\ \boldsymbol{\Phi}_{\boldsymbol{x}}(t_0) \end{pmatrix} = \begin{pmatrix} \boldsymbol{x}_0 \\ \mathbb{1}_{2n} \end{pmatrix},$$

where $D_{\boldsymbol{x}}\mathcal{F}(\boldsymbol{x})$ is the Jacobian matrix of $\mathcal{F}$ and $\mathbb{1}_{2n}$ is the $2n \times 2n$ identity matrix. Because $\boldsymbol{x}_0$ is a stationary point, $A = D_{\boldsymbol{x}}\mathcal{F}(\boldsymbol{x}) = D_{\boldsymbol{x}}\mathcal{F}(\boldsymbol{x}_0)$ is independent of time and

$$\boldsymbol{\Phi}_{\boldsymbol{x}_0}(t) = e^{At}. \tag{S1}$$

The fundamental matrix allows us to find the time evolution of a variation over the initial condition $\delta\boldsymbol{x}_0$. Specifically,

$$\delta\boldsymbol{x}(t) = \boldsymbol{\Phi}_{\boldsymbol{x}_0}(t)\,\delta\boldsymbol{x}_0 = e^{At}\,\delta\boldsymbol{x}_0. \tag{S2}$$

Employing the spectral norm $\|\boldsymbol{\Phi}_{\boldsymbol{x}_0}(t)\|$ [2] (the square root of the largest eigenvalue of the matrix $\boldsymbol{\Phi}_{\boldsymbol{x}_0}^{\dagger}\boldsymbol{\Phi}_{\boldsymbol{x}_0}$), one gets [1],

$$\lambda = \lim_{t\to\infty} \frac{1}{t} \log \|e^{At}\|. \tag{S3}$$

This limit can be expressed in terms of the eigenvalues λ_i of the matrix A. Denoting the maximum of the real parts of the eigenvalues of A by $\lambda_{\max}(A) = \max_i \mathrm{Re}\,(\lambda_i)$, we have that

$$\lambda = \lambda_{\max}(A). \tag{S4}$$

Proof. This proof was modeled after a discussion in [3].

First, note that both sides of Eq. (S4) are invariant under arbitrary basis changes. For any $A' = PAP^{-1}$, being P any invertible complex matrix, as both A and A' share the same eigenvalues, on the right hand side of Eq. (S4), $\lambda_{\max}(A) = \lambda_{\max}(A')$. On the other side of Eq. (S4), using the submultiplicativity of the spectral norm, we have

$$\left| \log \|e^{At}\| - \log \|e^{A't}\| \right| \le \log\bigl(\|P\|\|P^{-1}\|\bigr),$$

and then

$$\lim_{t\to\infty} \frac{1}{t} \log \|e^{At}\| = \lim_{t\to\infty} \frac{1}{t} \log \|e^{A't}\|.$$

Because of the above, we can write A in Jordan normal form $A = \mathrm{diag}(J_1, J_2, ..., J_N)$, where each Jordan block J_i corresponds to an eigenvalue λ_i of A with multiplicity n_i and is given by $J_i = \lambda_i \mathbb{1}_{n_i} + S_{n_i}$. Here, S_{n_i} is the $n_i \times n_i$ matrix with superdiagonal elements equal to one and zero elsewhere. We then get

$$\|e^{At}\| = \|\mathrm{diag}(e^{J_1 t}, e^{J_2 t}, ..., e^{J_N t})\| = \max_i \|e^{J_i t}\|,$$

so

$$\lim_{t\to\infty} \frac{1}{t} \log \|e^{At}\| = \max_i \left(\lim_{t\to\infty} \frac{1}{t} \log \|e^{J_i t}\| \right). \tag{S5}$$

Since the matrices $\lambda_i \mathbb{1}_{n_i}$ and S_{n_i} commute,

$$e^{J_i t} = e^{\lambda_i \mathbb{1}_{n_i} t} e^{S_{n_i} t} = e^{\lambda_i t} \sum_{k=0}^{n_i-1} \frac{t^k}{k!} S_{n_i}^k,$$

with spectral norm

$$\left\| e^{J_i t} \right\| = e^{\mathrm{Re}(\lambda_i) t} \left\| \sum_{k=0}^{n_i-1} \frac{t^k}{k!} S_{n_i}^k \right\|.$$

Thus,

$$\lim_{t\to\infty} \frac{1}{t} \log \left\| e^{J_i t} \right\| = \mathrm{Re}(\lambda_i) \qquad (S6)$$
$$+ \lim_{t\to\infty} \frac{1}{t} \log \left\| \sum_{k=0}^{n_i-1} \frac{t^k}{k!} S_{n_i}^k \right\|.$$

To complete the proof we have to show that the last term in Eq. (S6) equals zero. If $n_i = 1$, it is trivial, so assume $n_i > 1$. Using the triangle inequality of the norm and the fact that $\left\| S_{n_i}^k \right\| = 1$ for all $k \in \{0, 1, ..., n_i - 1\}$, we find the bounds

$$p_L(t) \le \left\| \sum_{k=0}^{n_i-1} \frac{t^k}{k!} S_{n_i}^k \right\| \le p_R(t), \qquad (S7)$$

where

$$p_L(t) = \frac{t^{n_i-1}}{(n_i-1)!} - \sum_{k=0}^{n_i-2} \frac{t^k}{k!}, \qquad p_R(t) = \sum_{k=0}^{n_i-1} \frac{t^k}{k!}.$$

For large enough t, $p_L(t) > 0$, and we may take the logarithm and divide by t the three terms in Eq. (S7). But for any real polynomial $p(t)$ with positive leading coefficient, one has $\lim_{t\to\infty} \frac{\log p(t)}{t} = 0$ by applying L'Hôpital's rule. Thus, using the squeeze theorem in Eq. (S7), we get

$$\lim_{t\to\infty} \frac{1}{t} \log \left\| \sum_{k=0}^{n_i-1} \frac{t^k}{k!} S_{n_i}^k \right\| = 0. \qquad (S8)$$

With Eq. (S5), Eq. (S6), and Eq. (S8), we arrive at the desired result,

$$\lim_{t\to\infty} \frac{1}{t} \log \left\| e^{At} \right\| = \max_i \mathrm{Re}(\lambda_i) = \lambda_{\max}(A). \qquad (S9)$$

Notice that we did not use any particular property of the matrix A at any point. This formula is true for any complex matrix A. $\qquad \square$

In what follows we apply this result to obtain the LEs for the classical simple pendulum, the Lipkin-Meshkov-Glick (LMG) model, and the Dicke model.

Lyapunov exponent of the simple pendulum

The Hamiltonian of the classical simple pendulum is

$$H(\theta, p_\theta) = \frac{p_\theta^2}{2ml^2} + mgl(1 - \cos\theta), \qquad (S10)$$

where m and l are the mass and length of the pendulum, respectively, g is the gravity acceleration, θ is the angle of the pendulum measured from the vertical, and $p_\theta = ml^2\dot{\theta}$ is the canonical momentum associated with θ. The Hamilton equations are $\dot{\boldsymbol{x}} = \boldsymbol{\mathcal{F}}(\boldsymbol{x}) = (\partial_{p_\theta} H, -\partial_\theta H)$ with $\boldsymbol{x} = (\theta, p_\theta)$. This model has two stationary points, $\boldsymbol{x}_\downarrow = (0, 0)$ at the bottom and $\boldsymbol{x}_\uparrow = (\pi, 0)$ at the top. The Jacobian matrix for each point can be obtained by simple differentiation,

$$A = \frac{1}{ml^2} \begin{pmatrix} 0 & 1 \\ \mp\omega^2 & 0 \end{pmatrix},$$

where $\omega = \sqrt{g/l}$, the negative sign corresponds to $\boldsymbol{x}_\downarrow$ and the positive sign to $\boldsymbol{x}_\uparrow$. For $\boldsymbol{x}_\downarrow$, the eigenvalues of A are pure imaginary numbers. From Eq. (S4), $\boldsymbol{x}_\downarrow$ is then a center point with zero LE, $\lambda_\downarrow = 0$, that is, it is a stable point. For $\boldsymbol{x}_\uparrow$, the eigenvalues of A are $\pm\omega$. This is a hyperbolic point with $\lambda_\uparrow = \omega$, so it is an unstable point. Despite being the go-to example of an integrable system, even the simple pendulum has a non-zero LE at $\boldsymbol{x}_\uparrow$. Yet, the system cannot be classified as chaotic, because this is an isolated point in the phase space.

Lyapunov exponent of the Lipkin-Meshkov-Glick model

To find the stationary points of the LMG model, we use the equations of motion for H_{LMG} (see this Hamiltonian in Eq. (2) of the main text), which are

$$\dot{Q} = \frac{\partial H_{\mathrm{LMG}}}{\partial P} = P\left(\Omega - \frac{\xi Q^2}{2}\right) \qquad (S11)$$

$$\dot{P} = -\frac{\partial H_{\mathrm{LMG}}}{\partial Q} = Q\left(\frac{\xi P^2}{2} - (2\xi + \Omega)\right) + \xi Q^3. \qquad (S12)$$

The stationary point happens at $\boldsymbol{x}_0 = (Q = 0, P = 0)$, where the Jacobian matrix is

$$A = \begin{pmatrix} 0 & \Omega \\ -(\Omega + 2\xi) & 0 \end{pmatrix}. \qquad (S13)$$

Its eigenvalues are $\lambda_\pm = \pm\sqrt{-(\Omega^2 + 2\xi\Omega)}$. According to Eq. (S4), the LE for this stationary point is zero for $\Omega \ge -2\xi$, because all the eigenvalues of A are imaginary. However, for $\Omega < -2\xi$, both eigenvalues of A are real and the LE equals the positive one. We then have

$$\lambda = \begin{cases} 0 & \text{if } \Omega \ge -2\xi \\ \sqrt{-(\Omega^2 + 2\Omega\xi)} & \text{if } \Omega < -2\xi \end{cases}. \qquad (S14)$$

Lyapunov exponent of the Dicke model

The Dicke model has a ground-state quantum phase transition (QPT) [4, 5] at

$$\omega_{0c} = \frac{4\gamma^2}{\omega}. \qquad (S15)$$

It is in the normal phase when $\omega_0 > \omega_{0c}$ and in the superradiant when $\omega_0 < \omega_{0c}$.

The Hamilton equations of the Dicke model have several stationary points depending on the set of Hamiltonian parameters that are chosen (see details in Refs. [5, 6]). We are interested in the unstable stationary point, which is related with the excited state quantum phase transition (ESQPT). In the classical phase space, this point is $\boldsymbol{x}_0 = (q, Q, p, P) = (0, 0, 0, 0)$, which, according to the classical Hamiltonian given in Eq. (4) of the main text, implies energy $-\omega_0$. In the normal phase, this point is stable and corresponds to the quantum ground state in the thermodynamic limit. Keeping ω and γ of the Dicke Hamiltonian constant (see the main text), this point becomes unstable, if one decreases the atomic level spacing, so that $\omega_0 < \omega_{0c}$ [4].

The Jacobian matrix at $\boldsymbol{x}_0$ is

$$A = \begin{pmatrix} 0 & 0 & \omega_0 & 0 \\ 0 & 0 & 0 & \omega \\ -\omega_0 & -2\gamma & 0 & 0 \\ -2\gamma & -\omega & 0 & 0 \end{pmatrix}, \qquad (S16)$$

and has the following eigenvalues

$$\lambda_{1,2,3,4} = \pm\frac{1}{\sqrt{2}}\sqrt{-(\omega^2 + \omega_0^2) \pm \sqrt{(\omega^2 - \omega_0^2)^2 + 16\gamma^2\omega\omega_0}}. \qquad (S17)$$

If $\omega_0 > \omega_{0c}$, all eigenvalues are imaginary and the LE is zero, but if $\omega_0 < \omega_{0c}$, some eigenvalues become real, and the largest one is given by

$$\lambda = \frac{1}{\sqrt{2}}\sqrt{-(\omega^2 + \omega_0^2) + \sqrt{(\omega^2 - \omega_0^2)^2 + 16\gamma^2\omega\omega_0}}. \qquad (S18)$$

FIDELITY OUT-OF-TIME ORDER CORRELATOR

The out-of-time order correlator (OTOC) is defined as

$$F(t) = \langle \hat{W}^\dagger(t)\hat{V}^\dagger\hat{W}(t)\hat{V}\rangle, \qquad (S19)$$

where $\hat{W}(t) = e^{i\hat{H}t}\hat{W}e^{-i\hat{H}t}$. If $\hat{W}$ and $\hat{V}$ are both unitary operators,

$$\mathrm{Re}(F(t)) = 1 - \langle \left[\hat{W}, \hat{V}\right]^\dagger \left[\hat{W}, \hat{V}\right]\rangle/2. \qquad (S20)$$

In Ref. [7], the fidelity OTOC (FOTOC) is obtained by using as operators

$$\hat{W} = e^{i\delta\phi\hat{G}}, \qquad (S21)$$

where $\hat{G}$ is a Hermitian operator and $\delta\phi$ is a perturbative small parameter, and

$$\hat{V} = |\Psi_0\rangle\langle\Psi_0|, \qquad (S22)$$

which is the projector onto the initial state $|\Psi_0\rangle$. With this choice of $\hat{V}$, Eq. (S20) becomes

$$1 - \mathrm{Re}(F(t)) = \langle \left[\hat{W}, \hat{V}\right]^\dagger \left[\hat{W}, \hat{V}\right]\rangle, \qquad (S23)$$

where this $F(t)$ is known as FOTOC. Using the following expansion up to second order in $\delta\phi$,

$$\langle\Psi_0|\hat{W}(t)|\Psi_0\rangle \approx 1 + i\delta\phi\langle\hat{G}(t)\rangle - \frac{\delta\phi^2}{2}\langle\hat{G}(t)^2\rangle, \qquad (S24)$$

it can be shown that $F(t)$ is related with the variance of $\hat{G}$ as

$$\frac{1 - F(t)}{(\delta\phi)^2} \approx (\langle\hat{G}(t)^2\rangle - \langle\hat{G}(t)\rangle^2) \equiv \sigma_G^2(t). \qquad (S25)$$

Since the evolution of $F(t)$ is equivalent to that of $\sigma_G^2(t)$, we refer to the variance as FOTOC.

For most interacting many-body systems the OTOCs must be calculated numerically. To do so for time-independent Hamiltonians, one employs the eigenbasis expansion. The FOTOC is then calculated as

$$\sigma_{\hat{G}}^2(t) = \sum_{i,j,k} c_j^{0*}c_i^0 e^{i(E_j - E_i)t}G_{jk}G_{ki} - \qquad (S26)$$

$$\left(\sum_{i,j} c_j^{0*}c_i^0 e^{i(E_j - E_i)t}G_{ji}\right)^2,$$

where $G_{ij} = \langle E_i|\hat{G}|E_j\rangle$, the energy eigenstate is $E_i\rangle$, and $c_i^0 = \langle\Psi_0|E_i\rangle$. Even though Eq. (S27) is formally simple, it is, in general, numerically challenging for non-integrable systems, such as the Dicke model. In this case, to deal with large system sizes, we resort to the truncated Wigner approximation (TWA), which is a phase space method.

TRUNCATED WIGNER APPROXIMATION IN THE DICKE MODEL

The calculation of the FOTOC, $\sigma_{x_i}^2 = \langle\hat{x}_i^2\rangle - \langle\hat{x}_i\rangle^2$, is reduced to obtaining the expectation value of powers of the canonical coordinates $\hat{x}_i$ of a quantum system under the short time evolution of a certain quantum state $|\Psi_0\rangle$. To do this, we use the TWA.

Consider the Wigner function [8] of the evolved initial state, $W(\boldsymbol{x}, t)$. The expectation value of an observable $\hat{O}$ may be calculated by

$$\langle\hat{O}(t)\rangle = \int W(\boldsymbol{x}, t)O(\boldsymbol{x})\mathrm{d}\boldsymbol{x},$$

where $O(\boldsymbol{x})$ is a function of the phase space variables known as the Weyl symbol of $\hat{O}$ [9]. In our case, the observables

of interest are $\hat{O} = \hat{x}_i^n$ with $n = 1, 2$. Their Weyl symbols, in very good approximation (the error is of order j^{-1}), are obtained by removing the hats off the observable $O = x_i^n$. Thus,

$$\langle x_i^n(t)\rangle = \int W(\boldsymbol{x}, t) x_i^n \mathrm{d}\boldsymbol{x}. \qquad (S27)$$

The TWA is used to deal with the evolution of the Wigner function [10, 11]. The idea of the approximation is to treat a positive Wigner function as a classical phase space distribution for short times, assuming that it remains constant over the classical phase space trajectories. The temporal evolution is then given by [12]

$$W(\boldsymbol{x}, t) = W(\boldsymbol{x}(-t), 0), \qquad (S28)$$

where $\boldsymbol{x}(t)$ is the classical trajectory in the classical Hamiltonian phase space. Inserting this in Eq. (S27), we get

$$\langle x_i^n(t)\rangle = \int W(\boldsymbol{x})\, x_i(t)^n \,\mathrm{d}\boldsymbol{x}. \qquad (S29)$$

Dicke model: TWA-quantum correspondence

For the Dicke model, we use the product of Glauber $|\alpha\rangle$ and Bloch $|z\rangle$ coherent states of the Heisenberg-Weyl and the SU(2) spaces, respectively, as initial states [13]. The Wigner function for these states is everywhere positive.

For Glauber states, the Wigner function is given by a normal distribution [14]

$$W_{q_0, p_0}(q, p) = \frac{j}{\pi} e^{-j\Delta^2}, \qquad (S30)$$

where $\Delta = \sqrt{(q - q_0)^2 + (p - p_0)^2}$ is the distance between (q, p) and (q_0, p_0).

For a Bloch coherent state, the Wigner function may be written as a sum of Legendre polynomials $P_k(x)$ [15, 16]

$$W_{\theta_0, \phi_0}(\theta, \phi) = \frac{(2j)!}{4\pi} \sum_{k=0}^{2j} \sqrt{\frac{(2k+1)}{(2j-k)!(2j+k+1)!}} P_k(\cos\Theta), \qquad (S31)$$

where $z = \tan(\theta/2)e^{i\phi}$ and Θ is the angle between (θ, ϕ) and (θ_0, ϕ_0) obtained from

$$\cos\Theta = \cos\theta\cos\theta_0 + \sin\theta\sin\theta_0\cos(\phi - \phi_0).$$

As j increases, Eq. (S31) converges rapidly to a normal distribution on the Bloch sphere

$$W_{\theta_0, \phi_0}(\theta, \phi) \approx \frac{j}{\pi} e^{-j\Theta^2}. \qquad (S32)$$

The Wigner function of a Dicke coherent state centered at $\boldsymbol{x_0}$ is given by the product of the Glauber and Bloch Wigner functions

$$W_{\boldsymbol{x_0}}(\boldsymbol{x}) = \left(\frac{j}{\pi}\right)^2 e^{-j(\Delta^2 + \Theta^2)}. \qquad (S33)$$
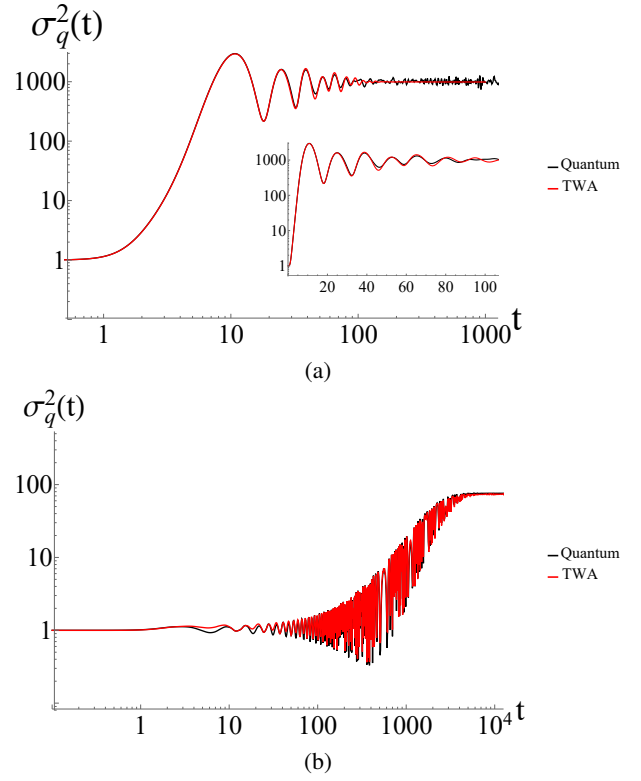

Figure 4. (Color online) FOTOC for the observable $\hat{q}$ in the Dicke model. The coherent state has (a) energy $E = -\omega_0 j$ centered at the stationary point $\boldsymbol{x_0} = (q = 0, p = 0, Q = 0, P = 0)$ and (b) $E = -2.5 j\omega_0$ centered in a regular point $\boldsymbol{x} = (q = -1.722, p = 0, Q = 1.2, P = 0)$. In both panels, the parameters are the experimental values used in Ref. [7, 18]: $\omega_0 = 0.649$, $\omega = 0.5$, $\gamma = 0.66$, and $j = 100$. The black line corresponds to the actual quantum evolution, while the red line is the truncated Wigner approximation. The inset in panel (a) shows the same data, but in a lin-log scale.

To compute the integral in Eq. (S29) with this initial Wigner function, we use a Monte Carlo method [17], where we sample a set ($\sim 10^4$) of initial conditions $\boldsymbol{x}$ from the initial normal Wigner distribution in Eq. (S33) and then calculate the mean of the values of x_i^n after evolving the points according to the classical Hamiltonian. The approximation in Eq. (S32) allows us to simplify the sampling from the distribution and save computational resources.

In Fig. 4, we compare the temporal TWA evolution with the exact quantum evolution in the Dicke model to determine where they diverge. We calculate the FOTOC of the observable $\hat{q}$ for a coherent state located at the critical point $\boldsymbol{x_0}$ for a given value of ω_0. The results are shown in Fig. 4 (a). Notice that there is perfect agreement for times beyond the exponential growth of the variance, providing a solid foundation to use this approximation to analyze the short time quantum behavior of the FOTOC, as we do in the main text.

Interestingly, this semiclassical approximation holds for even longer times in the regular case. This is seen in Fig. 4 (b), where we compare the TWA and the exact quantum evolution for a coherent state located in a regular region of the phase

space. In this case, we select a lower energy $E/j\omega_0 = -2.5$ and a point with $\boldsymbol{x} = (q = -1.722, p = 0, Q = 1.2, P = 0)$. We choose this point because it is located roughly at the center of the available phase space that is completely regular at this energy. The agreement between the semi-classical and quantum simulations lasts for a long time.

---

[1] Pierre Gaspard, <u>Chaos, scattering and statistical mechanics</u> (Cambridge Univ. Press, 1998).

[2] Roger A. Horn and Charles R. Johnson, "Norms for vectors and matrices," in <u>Matrix Analysis</u> (Cambridge University Press, 1985) pp. 257–342.

[3] Jack Dale, "Limit of log of norm of exponential of Hamiltonian matrix equals maximal eigenvalue," Mathematics Stack Exchange, url:https://math.stackexchange.com/q/3316285 (version: 2019-08-14), https://math.stackexchange.com/q/3316285.

[4] Michal Kloc, Pavel Stránský, and Pavel Cejnar, "Quantum phases and entanglement properties of an extended Dicke model," Ann. Phys. **382**, 85 – 111 (2017).

[5] M A Bastarrachea-Magnani, S Lerma-Hernández, and J G Hirsch, "Thermal and quantum phase transitions in atom-field systems: a microcanonical analysis," J. Stat. Mech. **2016**, 093105 (2016).

[6] M. A. Bastarrachea-Magnani, S. Lerma-Hernández, and J. G. Hirsch, "Comparative quantum and semiclassical analysis of atom-field systems. I. Density of states and excited-state quantum phase transitions," Phys. Rev. A **89**, 032101 (2014).

[7] R. J. Lewis-Swan, A. Safavi-Naini, J. J. Bollinger, and A. M. Rey, "Unifying scrambling, thermalization and entanglement through measurement of fidelity out-of-time-order correlators in the dicke model," Nature Communications **10**, 1581 (2019).

[8] E. Wigner, "On the quantum correction for thermodynamic equilibrium," Phys. Rev. **40**, 749–759 (1932).

[9] H. Weyl, "Quantenmechanik und gruppentheorie," Zeitschrift für Physik **46**, 1–46 (1927).

[10] M. J. Steel and M. J. Collett, "Quantum state of two trapped Bose-Einstein condensates with a josephson coupling," Phys. Rev. A **57**, 2920–2930 (1998).

[11] P.B. Blakie, A.S. Bradley, M.J. Davis, R.J. Ballagh, and C.W. Gardiner, "Dynamics and statistical mechanics of ultra-cold bose gases using c-field techniques," Advances in Physics **57**, 363–455 (2008).

[12] T. Gorin, Tomaz Prosen, Thomas H. Seligman, and Marko Žnidarič, "Dynamics of Loschmidt echoes and fidelity decay," Phys. Rep. **435**, 33 – 156 (2006).

[13] Wei-Min Zhang, Da Hsuan Feng, and Robert Gilmore, "Coherent states: Theory and some applications," Rev. Mod. Phys. **62**, 867–927 (1990).

[14] William Case, "Wigner functions and weyl transforms for pedestrians," Am. J. Phys. **76**, 937–946 (2008).

[15] There is a typo in Eq. (2.14) of Ref. [16], which has been corrected here.

[16] Popo Yang, Iván F Valtierra, Andrei B Klimov, Shin-Tza Wu, Ray-Kuang Lee, Luis L Sánchez-Soto, and Gerd Leuchs, "The wigner flow on the sphere," Physica Scripta **94**, 044001 (2019).

[17] J. Schachenmayer, A. Pikovski, and A. M. Rey, "Many-body quantum spin dynamics with monte carlo trajectories on a discrete phase space," Phys. Rev. X **5**, 011022 (2015).

[18] A. Safavi-Naini, R. J. Lewis-Swan, J. G. Bohnet, M. Gärttner, K. A. Gilmore, J. E. Jordan, J. Cohn, J. K. Freericks, A. M. Rey, and J. J. Bollinger, "Verification of a many-ion simulator of the dicke model through slow quenches across a phase transition," Phys. Rev. Lett. **121**, 040503 (2018).